EDGE ARTICLE

Check for updates

All publication charges for this article have been paid for by the Royal Society of Chemistry

Crystallographic visualization of C3-hydrocarbon-induced structural transformation and guest encapsulation within a flexible coordination network

Shao-Jie Qin,†[a] Mohana Shivanna,†[b] Mei-Yan Gao,[b] Cheng-Hua Deng, [b] Shi-Qiang Wang, [b] Dan Li,[a] Shao-Dan Fu,[a] Shuai Qiu,[a] Bai-Qiao Song [*a] and Qing-Yuan Yang [*c]

Flexible coordination polymers that can self-adjust, *via* closed (nonporous) to open (porous) switching, to match the size/shape of guest molecules are of particular interest. Herein, we report that C3 hydrocarbons can trigger a flexible SIFSIX network, $[Cu(SiF_6)(L)_2]_n$ (L = 1,4-bis(1-imidazolyl)benzene), **SIFSIX-23-Cu**, to switch from nonporous to partially open phases at 298 K with different gate opening pressures (propyne < propylene < propane). The single-crystal X-ray diffraction (SCXRD) measurements have succeeded in the crystallographic visualization of the C3-induced closed-to-open switching and the binding sites of gas molecules confined in the open phases. The results unambiguously showed that the closed phase can undergo adaptive structural expansion upon sorption of different C3 molecules, and the conformational changes of L *via* rotation and contortion under gas loading are responsible for the structural transformation. The host–gas interactions are dominated by C−H⋯F hydrogen bonds between gas molecules and SiF_6^{2-} anions and the size-matched chelation of linear propyne by SiF_6^{2-} pairs results in the stronger binding strength of propyne over propylene (propane), leading to the selective sorption of propyne from binary and ternary C3 gas mixtures, as confirmed by breakthrough experiments. This work highlights the vital role of host–gas interactions in governing the structural transitions and affords an efficient strategy to design high-performance flexible sorbents for challenging gas recognition and sorption.

Introduction

In nature, enzymes can adapt the shape and size of their binding sites to accommodate specific substrates, inspiring the development of stimuli-responsive materials (SRMs) that cover a broad scope of compositions and functional properties.[1] SRMs in traditional porous solids remain scarce, presumably because most, such as activated carbons and zeolites, are rigid under ordinary conditions.[2] As a new generation of porous metal–organic materials (MOMs),[3,4] porous coordination polymers (PCPs)[5] or metal–organic frameworks (MOFs)[6] offer a high degree of diversity, modularity and tunability with respect to their architectures and functionalities.[7] An emerging class of porous SRMs is exemplified by "soft"[8] or flexible MOMs

(FMOMs)[9,10] that transform their structures, sometimes dramatically, when exposed to gases, liquids and/or vapors.[11–13] These transformations usually result from coordination geometry isomerization,[14–17] linker rotation/contortion,[18–22] subnet displacement (in catenated networks),[15] or other events.[23–26] Unlike rigid MOMs usually showing characteristic type I isotherms,[27] FMOMs often exhibit stepwise adsorption isotherms with visible inflections mostly associated with structural transformation.[28–36] Particularly, FMOMs switching between nonporous (closed) and highly porous (open) phases under external stimuli have attracted considerable attention,[14–16,37] as they show negligible gas adsorption before the gate-opening pressure but an abrupt increase in uptake once the gate is opened, *i.e.*, a stepped type F-IV isotherm.[20] Such isotherms can substantially improve the working capacity for gas storage,[14,20] and are also favorable for gas separation if gate opening is differentiated by adsorbate types.[35,38–40]

However, sorption isotherms of FMOMs offer limited information about gas–solid interactions.[41,42] Insights into the structural changes associated with gas-triggered gate opening behavior and the binding sites of gas molecules trapped in the

[a]*College of Materials and Chemistry & Chemical Engineering, Chengdu University of Technology, Chengdu 610059, China. E-mail: bqsong@cdut.edu.cn*

[b]*Department of Chemical Sciences and Bernal Institute, University of Limerick, Limerick V94 T9PX, Republic of Ireland*

[c]*School of Chemical Engineering and Technology, Xi'an Jiaotong University, Xi'an 710049, China. E-mail: qingyuan.yang@xjtu.edu.cn*

† These authors contributed equally.

channels are essential for elucidation of the gate-opening mechanism and the design of high-performance switching sorbents for specific gases.[13,43] Although different technologies including specialized IR and NMR spectroscopy,[44] *in situ* powder X-ray diffraction (PXRD)[45] and molecular modelling[46] have been developed, SCXRD is the most convincing approach,[47–50] as it can often provide unequivocal dynamic structural information relating to gate-opening flexibility and host–guest interactions at the molecular level.[18,51] However, to date, the relevant examples are limited in the literature mainly because of the added requirements of maintaining crystal singularity of FMOMs after activation and undergoing drastic structural changes and/or lack of suitable host–guest interactions to strongly bind the gas molecules onto the pore surface.[52]

Recently we reported a 3D switching SIFSIX network, $[Cu(SiF_6)(L)_2]_n$ (L = 1,4-bis(1-imidazolyl)benzene), **SIFSIX-23-Cu**,[37] which maintained its single-crystal nature even after activation and showed reversible closed-to-open switching induced by CO_2, N_2 and some solvents including H_2O (Fig. 1a). As part of our continuing efforts to understand host–guest interactions in flexible coordination networks, we now provide a detailed investigation of the structural changes induced by different C3 hydrocarbons in **SIFSIX-23-Cu** (Fig. 1b). We demonstrate C3 hydrocarbons (propyne: C_3H_4; propylene: C_3H_6; propane: C_3H_8) can induce the nonporous form of **SIFSIX-23-Cu** to switch to partially open phases, with distinctly different gate-opening pressures ($C_3H_4 < C_3H_6 < C_3H_8$), and adaptive structural expansions that are clearly visualized by single-crystal X-ray diffraction (SCXRD). SCXRD characterization also validated the origin of framework changes, and the binding sites of C3 molecules confined in the channels which confirmed

stronger binding affinity of C_3H_4 over C_3H_6 (C_3H_8), aligning with the results of breakthrough experiments.

Results and discussion

Synthesis and crystal structures

The crystals of **SIFSIX-23-Cu** were obtained using our previous procedures.[37] The thermogravimetric analysis (TGA) is similar to the previous result (Fig. S1) and the PXRD pattern is consistent with the calculated one (Fig. S2), validating the successful synthesis and the purity of the sample. Its structure is an analog of the reported dipyridyl-ligand-based rigid SIFSIX net with an underlying **pcu** topology,[53] but possessing undulating square CuL_2 grid layers (sql) pillared by SIFSIX anions in a *cis*-coordination mode.[54] The *anti*- and *syn*-conformers of biimidazolyl ligand *i.e.*, L(*anti*) and L(*syn*), coexist in a 1:1 ratio in the **sql** net, providing the prerequisite for structural flexibility. The network could experience several phase contractions along with the release of guests in the channels due to conformational changes of the biimidazolyl ligand *via* rotation and contortion, leading to a final closed phase with negligible porosity. This nonporous phase can reversibly return to the original porous phase *via* the capture of different guests, including some organic solvents, H_2O, CO_2 and N_2.

Single-component adsorption isotherms

The low-pressure sorption isotherms of C3 hydrocarbons were measured at different temperatures on the anhydrous phase, **SIFSIX-23-Cu-β1**. As expected, the adsorption of C3 by the nonporous β1 phase exhibited desirable stepped type F-IV
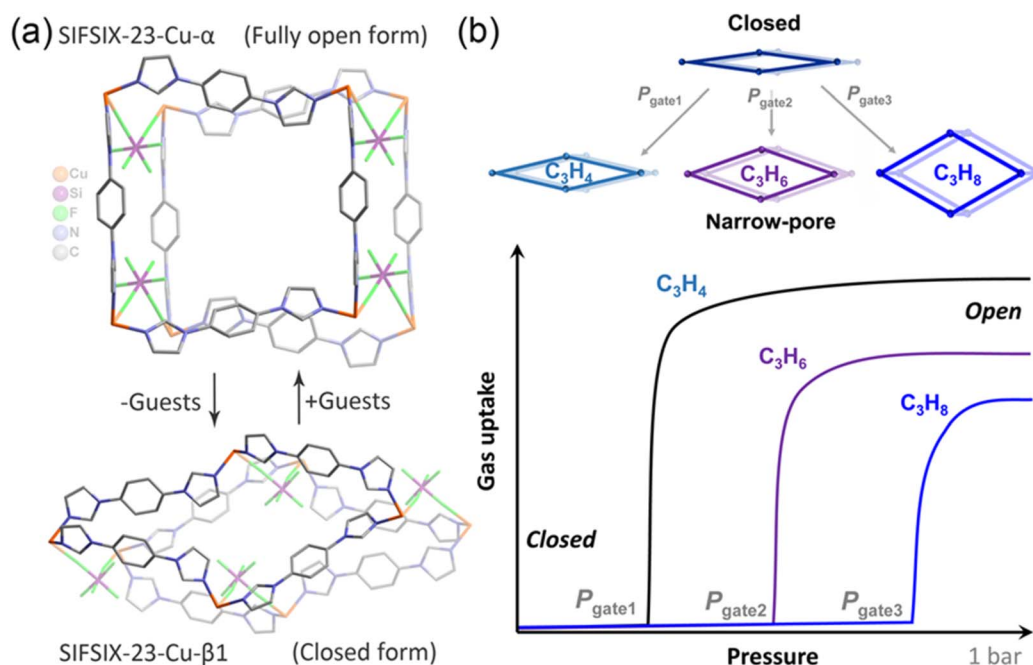

Fig. 1 (a) The structural transformation between the closed and open phases of a flexible SIFSIX network triggered by guest uptake/release. (b) The closed form shows adaptive pore opening for different C3 hydrocarbons, accompanied by stepwise adsorption isotherms with different gate-opening pressures.
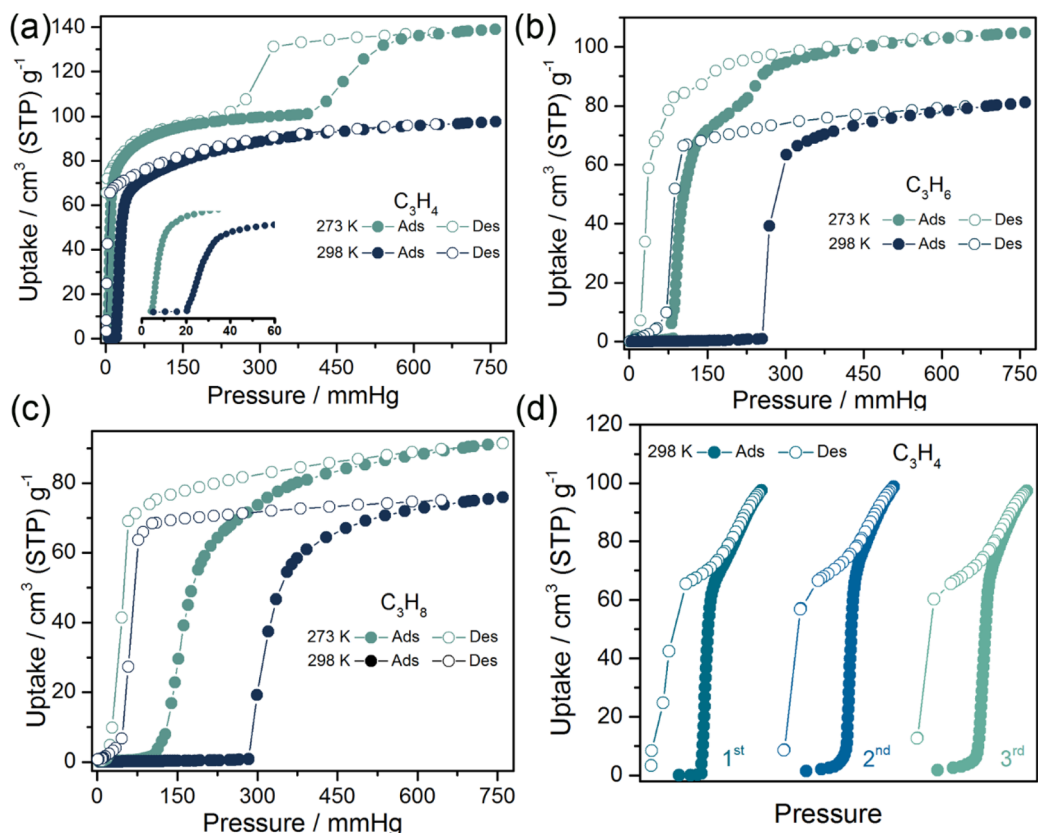
Fig. 2 The sorption isotherms recorded at 273 K and 298 K for (a) C_3H_4, (b) C_3H_6 and (c) C_3H_8. The inset in (a) highlights the low gate-opening pressures. (d) Three cycles of C_3H_4 sorption isotherms at 298 K.

isotherms with distinctly different gate-opening/closing pressures, indicative of gas-induced closed-to-open switching (Fig. 2). The pre-step uptakes for all the gases are negligible which is consistent with the nonporous feature of the β1 phase. For C_3H_4, the sudden gate opening with a threshold pressure of 20 mmHg at 298 K leads to a steep increase in uptake up to 97 cm^3 g^{-1} at 1 bar (Fig. 2a). The saturated adsorption capacity of C_3H_4 is higher than that of UTSA-200 (81.1 cm^3 g^{-1}),[55] ZNU-62 (82.0 cm^3 g^{-1}),[56] NKMOF-1-Ni (78.4 cm^3 g^{-1})[57] and TIFSIX-14-Cu-i (86.9 cm^3 g^{-1})[58] under similar conditions. Notably, the uptake of C_3H_4 at 0.1 bar (72.0 cm^3 g^{-1}) on **SIFSIX-23-Cu-β1** is even higher than the uptake of SIFSIX-3-Ni (66.8 cm^3 g^{-1}),[59] SIFSIX-3-Zn (50.6 cm^3 g^{-1}),[59] ELM-12 (61.4 cm^3 g^{-1}),[60] HOF-30a (59.8 cm^3 g^{-1})[61] and NbOFFIVE-1-Ni (42.3 cm^3 g^{-1})[59] at 1 bar, suggestive of the strong affinity for C_3H_4. At 273 K, the gate opening pressure was also <0.1 mmHg, but a second step was observed and the saturated uptake at 1 bar (139 cm^3 g^{-1}) was higher than that at 298 K. The second step suggests a further structural change. C_3H_6 and C_3H_8 induced gate opening of β1 with threshold pressures of 254.8 and 283.2 mmHg, and uptakes of 81.1 and 75.8 cm^3 g^{-1} at 298 K, respectively (Fig. 2b and c). The C_3H_6 and C_3H_8 sorption isotherms at 273 K were found to exhibit lower gate-opening pressures of 84.2 and 94.1 mmHg, and increased capacities of 104.9 and 89.3 cm^3 g^{-1}, respectively. Similar to C_3H_4, a second step was evident in the C_3H_6 sorption isotherm at low temperature but not in that of

C_3H_8. The pure gas sorption experiments revealed that the gate-opening pressures for C3 hydrocarbons increase in the following order: C_3H_4 < C_3H_6 < C_3H_8. Overall, the pure gas isotherms indicate that there are several open phases with various surface areas. Three cyclic C_3H_4 (298 K) sorption tests demonstrated the reversibility of the closed-to-open structural transition (Fig. 2d).

SCXRD studies of C3-induced structural transformations

To structurally elucidate the mechanism of gas-induced nonporous-to-porous switching with different gate-opening pressures and adsorption abilities in **SIFSIX-23-Cu**, we determined the crystal structures of **SIFSIX-23-Cu** loaded with C3 gas molecules, *i.e.*, **SIFSIX-23-Cu⊃C₃H₄**, **SIFSIX-23-Cu⊃C₃H₆** and **SIFSIX-23-Cu⊃C₃H₈**.

Single-crystal structure analysis directly revealed that the trapping of different hydrocarbons drove the gate opening of closed β1 to generate the related partially open phases, not the fully open phase α (Fig. 3a, S3 and S4). All the C3 molecule-loaded phases were crystallized in the $P\bar{1}$ space group (Tables S1 and S2). The observed closed-to-open transitions were fulfilled *via* hinge-like motions without changing the connectivity of the framework (Table S3). Although changes in Cu(II) geometry and SIFSIX configuration are small, the ∠Cu–Cu–Cu acute angle of the CuL₂ parallelogram unit of the **sql** net significantly increased (67.4–72.2° for C_3H_4–C_3H_8 *vs.* 46.7° in β1) (Fig. 2c),
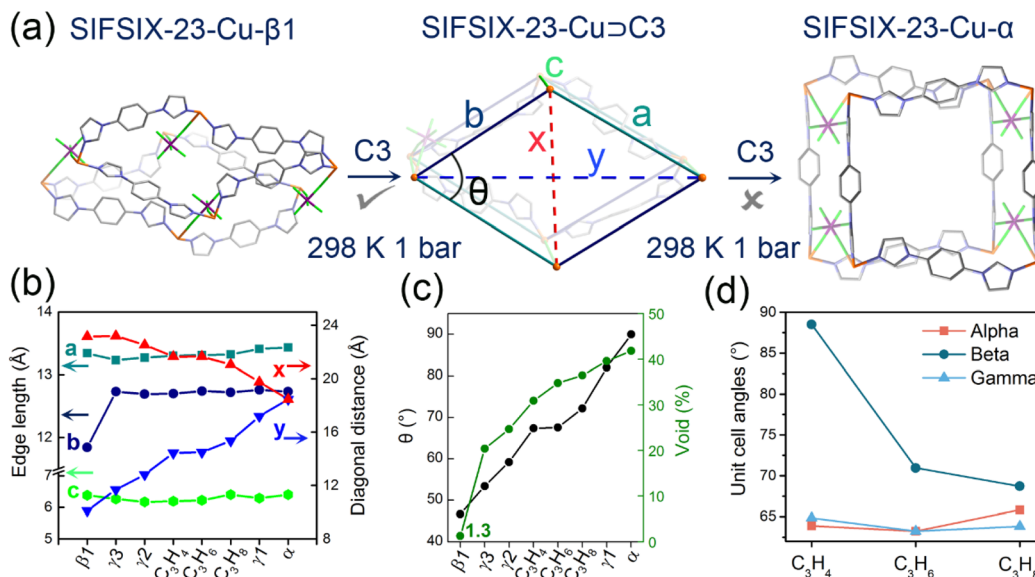
Fig. 3 (a) The closed phase β1 was triggered to partially open phases upon sorption of C3 hydrocarbons at 298 K, but the fully open phase α could not be reached even at pressures up to 1 bar. (b) Comparison of the edges of the simplified parallelepiped unit in (a) for different phases. (c) Comparison of the acute angles of the parallelograms in (a) and the void space for different phases. (d) Comparison of the unit cell angles for different C3-loaded forms.

accompanied by a slight shortening of the long diagonal (21.6–21.1 Å vs. 23.2 Å) and a striking lengthening of the short diagonal (14.4–15.4 Å vs. 10.1 Å in β1) (Fig. 2b). Meanwhile, the Cu–L(*anti*)–Cu edge of the parallelogram shows almost no change but on the contrary the Cu–L(*syn*)–Cu counterpart stretches (12.7 Å vs. 11.8 Å). The latter is due to a remarkable reduction in bending distortion of L(*syn*) (55.2° in β1 vs. <4.1° in gas-included phases) and the Cu–imidazolyl coordination junction (35.2° in β1 vs. <9.3°) (Fig. S5–S8). Notably, the free rotation of L including the swing of the imidazolyl ring and reorientation of the phenyl group was observed from β1 to the gas-included phase (Fig. S9–S12), which drives the structure deformation (a phenomenon particularly evident in L(*syn*) due to its 'angular' characteristic), accommodates the constraints and minimizes the lattice energy. In fact, previous theoretical calculations have proven that L possesses an intrinsically low rotation energy barrier (<13 kJ mol^{-1}) which is beneficial for the nonporous-to-porous switching observed here. The C–H···F hydrogen bonding between L and SIFSIX anions further stabilizes the structural changes and helps to maintain the single-crystal nature of gas-included phases (Table S4). The expansion of the framework results in an overall increase in the guest-accessible volume (1.3% (β1) vs. 30.9–36.5% (C_3H_4–C_3H_8)) as calculated by PLATON (Fig. 2c and S13).[62] The pore volumes of the open phase incorporating different guests at 298 K increase in the following sequence C_3H_4 < C_3H_6 < C_3H_8, which substantiates that guest-dependent closed-to-open switching can adjust the open phases to adapt to guests of different molecular sizes and geometries. Notably, although the ∠Cu–Cu–Cu acute angle and the edges of the CuL$_2$ parallelogram unit remain almost constant after loading C_3H_4 and C_3H_6, the differences in void space and unit cell parameters clearly prove

the self-adaptive feature of **SIFSIX-23-Cu-β1** to them (Fig. 3d and Table S2). It is noteworthy that **SIFSIX-23-Cu⊃C_3H_4** presents the highest C_3H_4 uptake but the smallest void space (after removal of C_3H_4) among C3 induced open phases, confirming the tight binding of C_3H_4 in the structure. Additionally, the C3 gas loaded phases are different from those previously discovered narrow pore forms (γ1–γ3), which contain H_2O and methanol as guests (Fig. S4 and Table S2), further confirming the guest-dependent structural expansion ability of β1. To our knowledge, direct SCXRD characterization of hydrocarbon-triggered structural switching from nonporous to porous phase is very rare.[52] The PXRD patterns of the nonporous phase (**SIFSIX-23-Cu-β1**) under 1 bar of each C3 gas collected at 298 K match well with those calculated from the SCXRD-determined crystal structures, confirming the accuracy of the SCXRD measurement procedures (Fig. S14).

SCXRD studies of guest binding

SCXRD characterization of gas-induced structural transformation can provide deep insights into the dynamic structural information at the molecular level, and additionally it can directly visualize the binding sites of gas molecules trapped in the channels, although this is challenging. Fortunately, the binding of C3 molecules in the gas-confined open phases of **SIFSIX-23-Cu** can be observed crystallographically (Fig. 4). For **SIFSIX-23-Cu⊃C_3H_4**, three distinct types of C_3H_4 molecules can be observed (Fig. 4a, S15 and S16). C_3H_4-I lies parallel to the CuL$_2$ plane (Fig. 4b), with its alkynyl end oriented towards two SIFSIX anions arranged along the Cu-L(*syn*)-Cu edge (SIFSIX pair 1) and bound to one of them *via* C–H···F hydrogen bonds (H···F = 2.587/2.893 Å). The methyl group points towards the channel center, with the molecular axis inclined at 53.8° to the
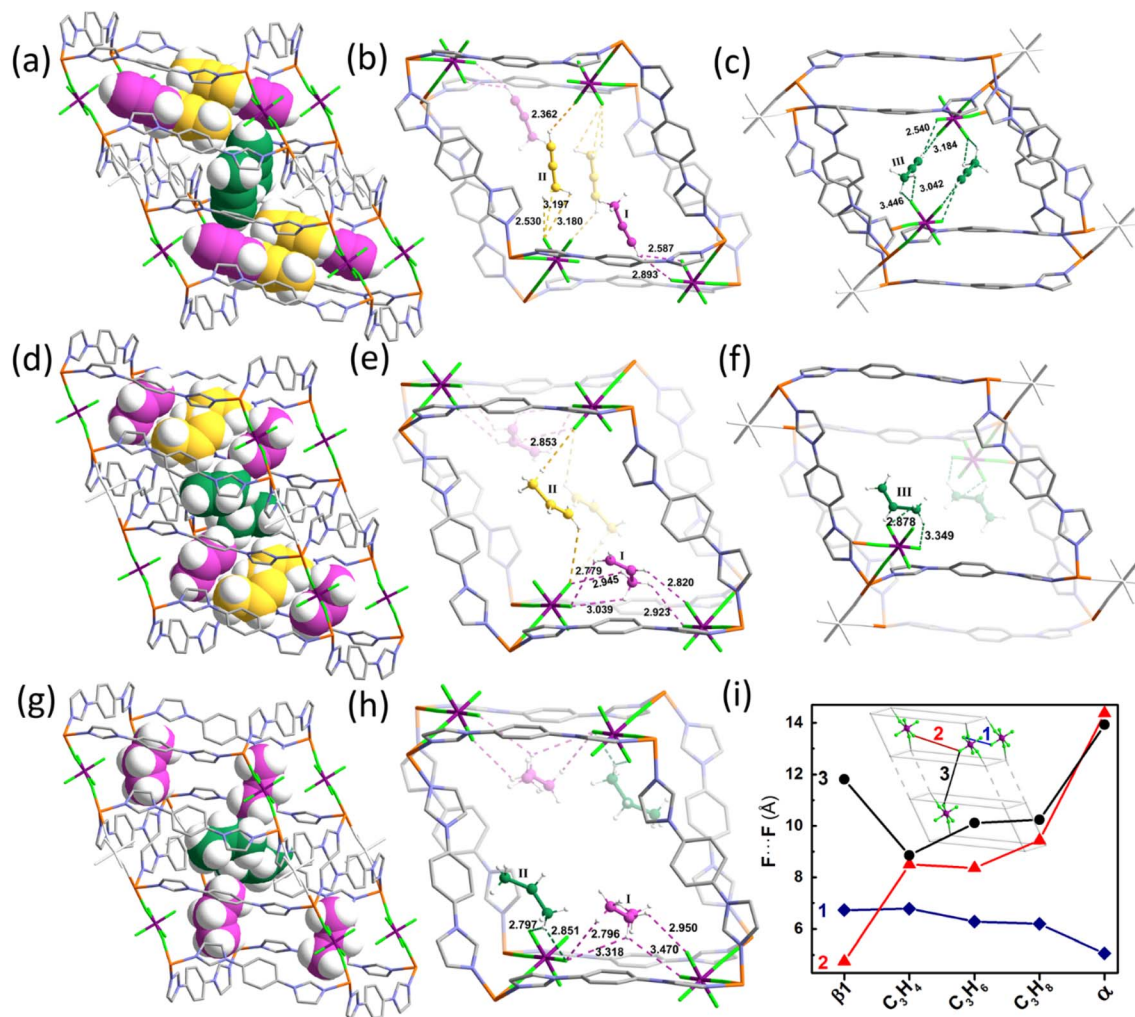
Fig. 4 Space filling representation of C_3H_4 (a), C_3H_6 (d) and C_3H_8 (g) molecules located in the structures. The C_3H_4 (b and c) and C_3H_6 (e and f) molecules residing inside the parallelepiped unit (b and e) and siting between parallelepiped units (c and f). (h) The C_3H_8 molecules in the structure. (i) The F···F distances of different SIFSIX pairs vary for different C3 loadings.

edge. C_3H_4-II lies parallel to the CuL_2 plane, nestled between two SIFSIX anions (SIFSIX pair 2) along the short diagonal of the CuL_2 parallelogram. The suitable F···F separation (8.504 Å) enables SIFSIX pair 2 to chelate C_3H_4-II in a head-on fashion *via* dual C–H···F hydrogen bonding interactions (H···F = 2.893 Å between the alkynyl end and anion, 2.530–3.197 Å between the methyl group and anion). C_3H_4-III is situated between two obtuse corners of adjacent cages, inclined at 30.5° to the CuL_2 plane (Fig. 4c). The two ends of C_3H_4-III are oriented towards two SIFSIX anions (SIFSIX pair 3) from neighboring cages, and are chelated by them *via* C–H···F hydrogen bonding interactions (H···F = 2.540/3.184 Å between the alkynyl end and anion, 3.042–3.446 Å between the methyl group and anion) due to the suitable F···F distance (8.860 Å).

Similarly, three different types of C_3H_6 can be discovered in **SIFSIX-23-Cu ⊃ C_3H_6** (Fig. 4d, S17 and S18). C_3H_6-I is chelated by SIFSIX pair 1 in a side-on manner *via* various C–H···F hydrogen bonding interactions (H···F = 2.779–3.039 Å). C_3H_6-II is chelated by SIFSIX pair 2 in a head-on fashion *via* C–H···F

hydrogen bonding interactions (H···F = 2.853/3.266 Å) (Fig. 4e). C_3H_6-III resides close to one obtuse corner of the cage and is bound to one anion of SIFSIX pair 3 *via* C–H···F hydrogen bonding interactions (H···F = 2.878/3.349 Å) (Fig. 4f). In **SIFSIX-23-Cu ⊃ C_3H_8**, two types of C_3H_8 molecules (C_3H_8-I and C_3H_8-II) are identified (Fig. 4g, S18 and S19), whose positions and binding manners are similar to those of C_3H_6-I and C_3H_6-III (H···F = 2.796–3.470 Å), respectively (Fig. 4h). Unlike C_3H_4-II and C_3H_6-II, no C_3H_8 molecule is chelated by SIFSIX pair 2, due to the very large SIFSIX···SIFSIX separation (F···F distance of 9.297 Å). In addition to the hydrogen bonds observed, there are numerous vdW and C–H···π interactions between C3 molecules and the aromatic rings of the framework (Fig. S16, S18 and S20). Based on the SCXRD results, the binding sites of C3 molecules are approximately similar, and guest-dependent non-porous-to-porous switching can generate open phases that match the size and geometry of guest molecules. It can be concluded that the binding of C_3H_4 is stronger than that of C_3H_6 and C_3H_8 by comparing the C–H···F hydrogen bonding distances and

binding modes, consistent with the results of sorption experiments (Fig. S21–S29). A comparison of the interionic distances in SIFSIX pairs 1, 2, and 3 across all C3-loaded structures reveals distinct trends that vary with different adsorbates (Fig. 4i). SIFSIX pair 1 shows minimal changes for the three sorbates, whereas SIFSIX pair 2 exhibits a similar changing tendency to the diagonal distance of CuL$_2$ (y in Fig. 3). Remarkably, SIFSIX pairs 2 and 3 change in opposite ways: for C$_3$H$_4$ and C$_3$H$_6$, pair 2 remains almost unchanged while pair 3 varies significantly; for C$_3$H$_6$ and C$_3$H$_8$, pair 2 changes substantially while pair 3 remains constant. This further confirmed that the host framework can self-adapt to accommodate different C3 molecules.

The guest–host and guest–guest interactions present in the C3-loaded structures were further analysed by means of Hirshfeld surfaces[63] and their corresponding fingerprint plots were documented. The d_{norm} surface of each structure clearly shows a different color distribution that discloses different levels of contacts/interactions (Fig. 5a, c and e). As shown in the decomposed 2D fingerprint plots (Fig. 5b, d and f), the contribution proportions of H···F interactions in the Hirshfeld surface area of C$_3$H$_4$ (11.6%) were higher than those of C$_3$H$_6$ and C$_3$H$_8$, indicating more hydrogen bonds between C$_3$H$_4$ and F atoms of SiF$_6^{2-}$ anions (Fig. S30–S32). Also, the positions of spikes in the H···F fingerprint plots suggest the distribution of scattering points in a very short (d_e, d_i) range for C$_3$H$_4$, suggesting the shortest H···F interactions in the C$_3$H$_4$-loaded structure and confirming the tight binding mode of C$_3$H$_4$. The shortest contact between C$_3$H$_4$ and SiF$_6^{2-}$ anions can also be

reflected by the distinct colors (red) in the d_{norm} surface of the Hirshfeld surface which is more apparent for C$_3$H$_4$ compared with C$_3$H$_6$ and C$_3$H$_8$. Given the chelating binding modes and the stronger hydrogen bonds between F atoms and the acidic alkynyl hydrogen atoms of C$_3$H$_4$, it can be inferred that the binding of C$_3$H$_4$ through H···F hydrogen bonds is stronger compared with C$_3$H$_6$ and C$_3$H$_8$. Additionally, the C···H/H···C short contacts are more pronounced for C$_3$H$_4$ (30%) compared to C$_3$H$_6$ and C$_3$H$_8$, further suggesting the tight binding fashion of C$_3$H$_4$ (Fig. 5b, d, and f). The H(alkyne)···C(host) contacts reveal the presence of C–H···π interactions between C3 gases and the host, especially between the methyl group of the gas molecule and the aromatic plane of ligand L (Fig. S16, S18 and S20). For all C3-loaded structures, there are numerous H···H short contacts, indicative of the ubiquitous vdW interactions. By carefully checking the d_{norm} surface for each structure, it can concluded that the guest–guest interactions also exist in all structures.

C$_3$H$_4$ selective sorption tests

The preferential and stronger binding affinity of C$_3$H$_4$ compared to C$_3$H$_6$ within **SIFSIX-23-Cu** was further investigated through quantitative fixed-bed column breakthrough experiments using binary gas mixtures of C$_3$H$_4$/C$_3$H$_6$ (40 : 60 and 10 : 90 v/v) at 298 K. Interestingly, the sample in the packed column underwent a color change gradually from light blue (activated β1 phase) to light purple (gas loaded phase), which evolved over
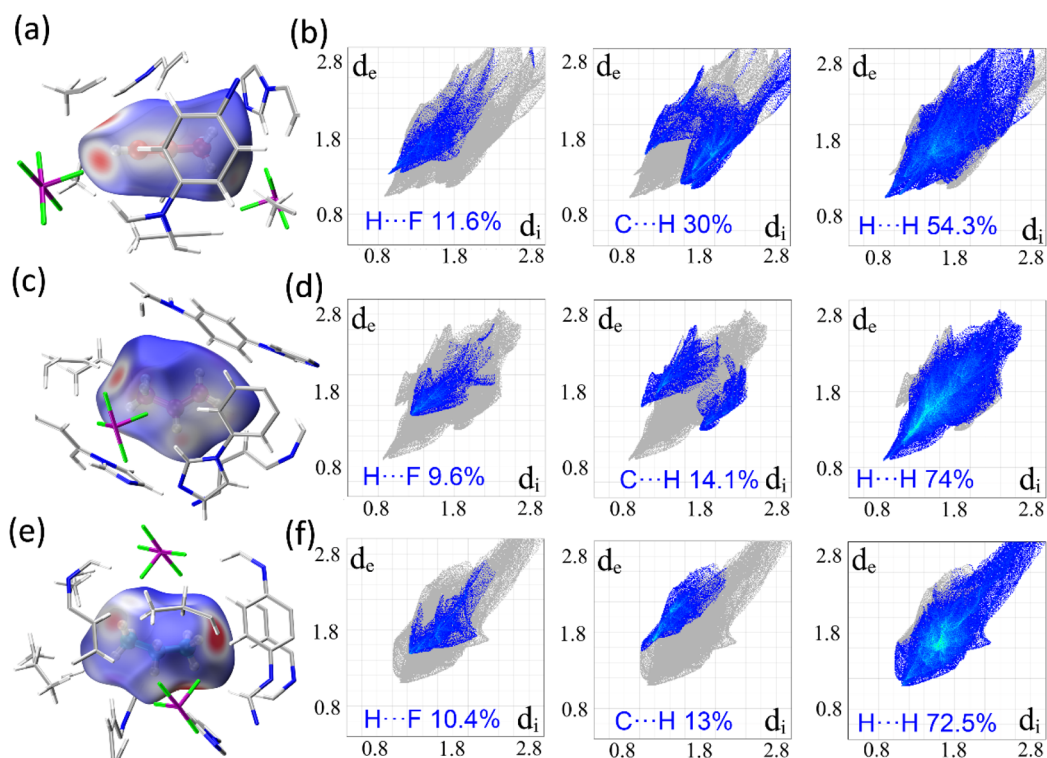

Fig. 5 (a, c and e) The Hirshfeld surface (d_{norm}) for one C$_3$H$_4$ (a), C$_3$H$_6$ (c) and C$_3$H$_8$ (e). The red (blue) spots represent the strong (weak) short-term contacts between neighbouring atoms. (b, d and f) The decomposed 2D fingerprint plots and proportion for the H···F, H···C/C···H and H···H contacts of the C$_3$H$_4$ (b), C$_3$H$_6$ (d) and C$_3$H$_8$ (f) molecules on the Hirshfeld surfaces.
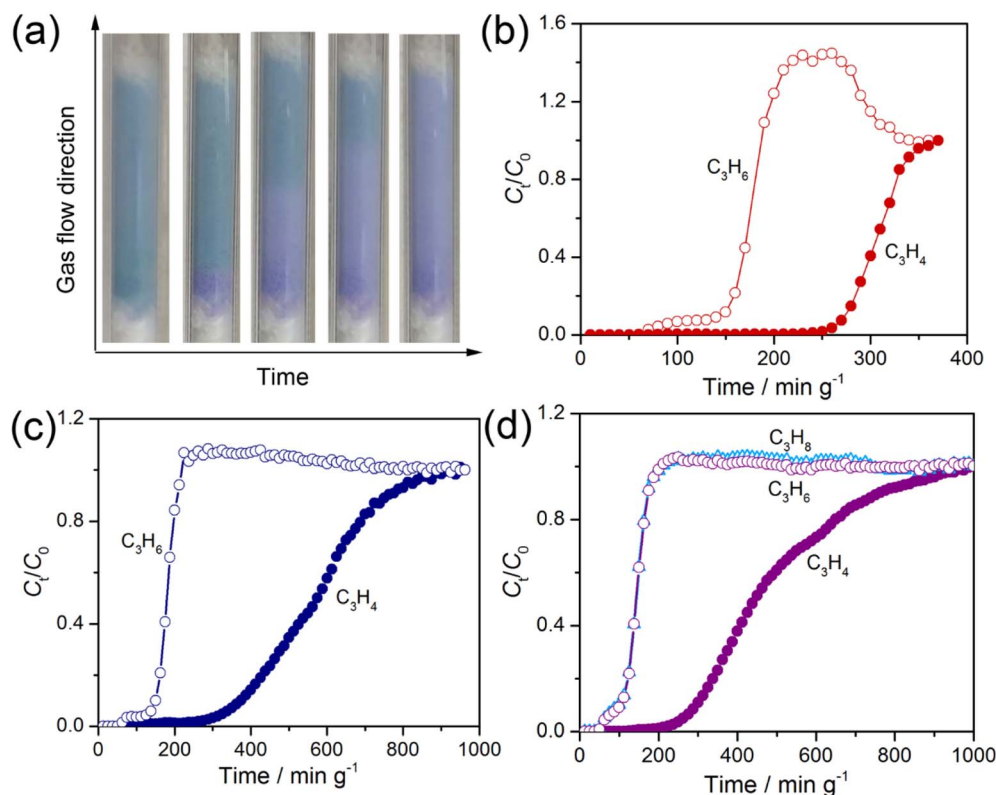
Fig. 6 (a) Sample was packed in the column and underwent a colour change along the gas flow direction over time. (b–d) Experimental breakthrough curves for 40/60 (v/v) and 10/90 (v/v) C_3H_4/C_3H_6 binary mixtures (b and c) and a 10/40/50 (v/v/v) C_3H_4/C_3H_6/C_3H_8 ternary mixture (d).

time along the gas flow direction during the breakthrough experiments (Fig. 6a), showcasing the uptake of the gas molecules from the mixture. As expected, C_3H_6 flowed out much earlier than C_3H_4 did, leading to a period of purely C_3H_6 leaving the column (Fig. 6b and c). However, the C_3H_6 flow rate (C_t/C_0) did not reach equilibrium directly like a non-adsorbing gas species but with a small step which is similar to that observed in adsorption isotherms, implying co-adsorption of C_3H_6 after gate-opening by C_3H_4 (Fig. S33 and S34). C_3H_4 were retained in the column for ca. 220 and 265 min g^{-1} with the adsorbed amounts of 3.93 and 1.18 mmol g^{-1} under 40 : 60 and 10 : 90 C_3H_4/C_3H_6 gas mixtures, respectively. The average C_3H_6 purities in the outlet gas streams were 98.5% (40 : 60) and 99.0% (10 : 90), respectively. Three consecutive cycles of breakthrough experiments (40 : 60 C_3H_4/C_3H_6) demonstrated the stability of the sample (Fig. S35), which was further validated by PXRD tests (Fig. S36). The desorption curves after the breakthrough experiment (10 : 90 C_3H_4/C_3H_6) indicated that heating was required to fully remove the adsorbed C_3H_4 molecules, suggestive of the stronger binding ability of C_3H_4 over C_3H_6 (Fig. S37). Notably, although under both conditions, the partial pressure for C_3H_6 can also trigger the gate opening behavior, SIFSIX-23-Cu still showed excellent separation performance which can probably be ascribed to the stronger binding interaction between C_3H_4 molecules and the host framework compared with that of C_3H_6, and the slow kinetics of C_3H_6-induced gate-opening behavior.

To further examine the potential of SIFSIX-23-Cu for the selective adsorption of C_3H_4 in the presence of both C_3H_6 and C_3H_8, a breakthrough experiment with a C_3H_4/C_3H_6/C_3H_8 (10 : 40 : 50 v/v/v) ternary gas mixture was conducted under similar conditions (Fig. 6d). We selected this specific gas composition to ensure that the partial pressure of C_3H_4 exceeded the gate-opening pressure observed in the single component isotherm but those of C_3H_6 and C_3H_8 lay below their gate-opening pressures even after C_3H_4 in the gas mixture is completely adsorbed, which can unveil the gate opening effect of C_3H_6 and C_3H_8 on the separation performance. Surprisingly, C_3H_6 and C_3H_8 broke out of the packed column simultaneously with a negligible step, confirming that SIFSIX-23-Cu can efficiently exclude C_3H_6 and C_3H_8 (Fig. 6), and co-adsorption seems to be partly suppressed in comparison with the corresponding binary mixture. In contrast, the retention time and adsorbed amount of C_3H_4 in the packed column are ca. 225 min g^{-1} and 1.0 mmol g^{-1}, close to those under the 10 : 90 C_3H_4/C_3H_6 mixture, which further confirmed that the gate opening effect from C_3H_6 does not significantly affect the selective adsorption of C_3H_4 from the mixture. The average concentration of C_3H_4 in the outlet is about 0.34%, suggestive of the effective removal of C_3H_4 from the ternary C3 mixture (Fig. S38). Similarly, heating was needed to completely desorb the strongly bound C_3H_4 molecules from the sorbent (Fig. S39). The observed good separation performance of SIFSIX-23-Cu can be attributed to the large difference

in gate-opening pressures for C_3H_4 over C_3H_6 (and C_3H_8) and the strength of the host–guest interactions once open.

Conclusions

In conclusion, we revealed the structural switching between nonporous and porous phases induced by C3 hydrocarbons in a flexible SIFSIX net. Sorption experiments and SCXRD experiments confirmed that the nonporous-to-porous structural switching is guest-dependent and can generate partially open phases that adapt to the size and geometry of C3 hydrocarbons. The binding sites for C3 molecules identified by SCXRD displayed stronger binding of C_3H_4 compared with C_3H_6 and C_3H_8, thus enhancing discrimination ability for the former. The selective adsorption of C_3H_4 from binary and ternary C3 gas mixtures was evaluated by experimental breakthrough tests. This work highlights the significant importance of host–guest interaction in the structural transformation and selective adsorption performance of FMOMs. Compared with the difficulty in fine-tuning the pore size and chemistry of rigid MOMs to differentiate gas species with similar properties, FMOMs switching from nonporous to guest-specific porous phases with different gate-opening pressures probably can be a potential approach to improve the recognition ability for challenging gas species.

Author contributions

S. J. Qin and M. Shivanna equally contributed to this work and carried out the synthesis, characterization, sorption and X-ray diffraction measurements, and writing – original draft; D. Li, S. D. Fu and S. Qiu assisted with the characterization analysis; M. Y. Gao, C. H. Deng and S. Q. Wang assisted with the gas sorption measurements and data analysis; B. Q. Song and Q. Y. Yang carried out the methodology, supervision, and writing – review & editing; all authors contributed to preparing the manuscript.

Conflicts of interest

The authors declare no competing financial interests.

Data availability

CCDC 2044415, 2044416 and 2034435 contain the supplementary crystallographic data for this paper.[64a–c]

The data supporting this article have been included as part of supplementary information (SI). Supplementary information: the experimental sections of materials and synthesis, the methods for the SCXRD measurements, the details for breakthrough tests, and the tables and figures. See DOI: https://doi.org/10.1039/d5sc07430d.

Acknowledgements

Notes and references

1 P. Theato, B. S. Sumerlin, R. K. O'Reilly and T. H. Epps III, *Chem. Soc. Rev.*, 2013, **42**, 7055–7056.

2 Y. Chai, X. Han, W. Li, S. Liu, S. Yao, C. Wang, W. Shi, I. da-Silva, P. Manuel, Y. Cheng, L. D. Daemen, A. J. Ramirez-Cuesta, C. C. Tang, L. Jiang, S. Yang, N. Guan and L. Li, *Science*, 2020, **368**, 1002–1006.

3 J. J. Perry Iv, J. A. Perman and M. J. Zaworotko, *Chem. Soc. Rev.*, 2009, **38**, 1400–1417.

4 Z. Chen, M. C. Wasson, R. J. Drout, L. Robison, K. B. Idrees, J. G. Knapp, F. A. Son, X. Zhang, W. Hierse, C. Kühn, S. Marx, B. Hernandez and O. K. Farha, *Faraday Discuss.*, 2021, **225**, 9–69.

5 S. Kitagawa, R. Kitaura and S.-i. Noro, *Angew. Chem., Int. Ed.*, 2004, **43**, 2334–2375.

6 H. Furukawa, K. E. Cordova, M. O'Keeffe and O. M. Yaghi, *Science*, 2013, **341**, 1230444.

7 S. Mukherjee and M. J. Zaworotko, *Trends Chem.*, 2020, **2**, 506–518.

8 S. Horike, S. Shimomura and S. Kitagawa, *Nat. Chem.*, 2009, **1**, 695–704.

9 G. Férey and C. Serre, *Chem. Soc. Rev.*, 2009, **38**, 1380–1399.

10 A. Schneemann, V. Bon, I. Schwedler, I. Senkovska, S. Kaskel and R. A. Fischer, *Chem. Soc. Rev.*, 2014, **43**, 6062–6096.

11 S. Krause, N. Hosono and S. Kitagawa, *Angew. Chem., Int. Ed.*, 2020, **59**, 15325–15341.

12 K. Koupepidou, A. Subanbekova and M. J. Zaworotko, *Chem. Commun.*, 2025, **61**, 3109–3126.

13 I. Senkovska, V. Bon, L. Abylgazina, M. Mendt, J. Berger, G. Kieslich, P. Petkov, J. Luiz Fiorio, J.-O. Joswig, T. Heine, L. Schaper, C. Bachetzky, R. Schmid, R. A. Fischer, A. Pöppl, E. Brunner and S. Kaskel, *Angew. Chem., Int. Ed.*, 2023, **62**, e202218076.

14 J. A. Mason, J. Oktawiec, M. K. Taylor, M. R. Hudson, J. Rodriguez, J. E. Bachman, M. I. Gonzalez, A. Cervellino, A. Guagliardi, C. M. Brown, P. L. Llewellyn, N. Masciocchi and J. R. Long, *Nature*, 2015, **527**, 357–361.

15 A.-X. Zhu, Q.-Y. Yang, A. Kumar, C. Crowley, S. Mukherjee, K.-J. Chen, S.-Q. Wang, D. O'Nolan, M. Shivanna and M. J. Zaworotko, *J. Am. Chem. Soc.*, 2018, **140**, 15572–15576.

16 M.-Y. Zhou, X.-W. Zhang, H. Yi, Z.-S. Wang, D.-D. Zhou, R.-B. Lin, J.-P. Zhang and X.-M. Chen, *J. Am. Chem. Soc.*, 2024, **146**, 12969–12975.

17 R. E. Morris and L. Brammer, *Chem. Soc. Rev.*, 2017, **46**, 5444–5462.

18 D. P. van Heerden, V. J. Smith, H. Aggarwal and L. J. Barbour, *Angew. Chem., Int. Ed.*, 2021, **60**, 13430–13435.

19 A. P. Katsoulidis, D. Antypov, G. F. S. Whitehead, E. J. Carrington, D. J. Adams, N. G. Berry, G. R. Darling, M. S. Dyer and M. J. Rosseinsky, *Nature*, 2019, **565**, 213–217.

20 Q.-Y. Yang, P. Lama, S. Sen, M. Lusi, K.-J. Chen, W.-Y. Gao, M. Shivanna, T. Pham, N. Hosono, S. Kusaka, J. J. Perry IV,

S. Ma, B. Space, L. J. Barbour, S. Kitagawa and M. J. Zaworotko, *Angew. Chem., Int. Ed.*, 2018, **57**, 5684–5689.

21 V. I. Nikolayenko, D. C. Castell, D. Sensharma, M. Shivanna, L. Loots, K. A. Forrest, C. J. Solanilla-Salinas, K.-i. Otake, S. Kitagawa and L. J. Barbour, *Nat. Chem.*, 2023, **15**, 542–549.

22 H. Fang, X.-Y. Liu, H.-J. Ding, M. Mulcair, B. Space, H. Huang, X.-W. Li, S.-M. Zhang, M.-H. Yu, Z. Chang and X.-H. Bu, *J. Am. Chem. Soc.*, 2024, **146**, 14357–14367.

23 C. Gu, N. Hosono, J.-J. Zheng, Y. Sato, S. Kusaka, S. Sakaki and S. Kitagawa, *Science*, 2019, **363**, 387–391.

24 H. Yang, T. X. Trieu, X. Zhao, Y. Wang, Y. Wang, P. Feng and X. Bu, *Angew. Chem., Int. Ed.*, 2019, **58**, 11757–11762.

25 S. K. Elsaidi, M. H. Mohamed, D. Banerjee and P. K. Thallapally, *Coord. Chem. Rev.*, 2018, **358**, 125–152.

26 S.-H. Lo, L. Feng, K. Tan, Z. Huang, S. Yuan, K.-Y. Wang, B.-H. Li, W.-L. Liu, G. S. Day, S. Tao, C.-C. Yang, T.-T. Luo, C.-H. Lin, S.-L. Wang, S. J. L. Billinge, K.-L. Lu, Y. J. Chabal, X. Zou and H.-C. Zhou, *Nat. Chem.*, 2020, **12**, 90–97.

27 R.-B. Lin, S. Xiang, W. Zhou and B. Chen, *Chem*, 2020, **6**, 337–363.

28 T. Kundu, M. Wahiduzzaman, B. B. Shah, G. Maurin and D. Zhao, *Angew. Chem., Int. Ed.*, 2019, **58**, 8073–8077.

29 H. Zeng, M. Xie, Y.-L. Huang, Y. Zhao, X.-J. Xie, J.-P. Bai, M.-Y. Wan, R. Krishna, W. Lu and D. Li, *Angew. Chem., Int. Ed.*, 2019, **58**, 8515–8519.

30 M.-H. Yu, B. Space, D. Franz, W. Zhou, C. He, L. Li, R. Krishna, Z. Chang, W. Li, T.-L. Hu and X.-H. Bu, *J. Am. Chem. Soc.*, 2019, **141**, 17703–17712.

31 J. Tian, Q. Chen, F. Jiang, D. Yuan and M. Hong, *Angew. Chem., Int. Ed.*, 2023, **62**, e202215253.

32 T. Xu, W. Jiang, Y. Tao, M. Abdellatief, K. E. Cordova and Y.-B. Zhang, *J. Am. Chem. Soc.*, 2024, **146**, 11225–11234.

33 L. Zhang, B. Yu, M. Wang, Y. Chen, Y. Wang, L.-B. Sun, Y.-B. Zhang, Z. Zhang, J. Li and L. Li, *Angew. Chem., Int. Ed.*, 2025, **64**, e202418853.

34 M. Shivanna, K.-i. Otake, S. Hiraide, T. Fujikawa, P. Wang, Y. Gu, H. Ashitani, S. Kawaguchi, Y. Kubota, M. T. Miyahara and S. Kitagawa, *Angew. Chem., Int. Ed.*, 2023, **62**, e202308438.

35 Z. Niu, Z. Fan, T. Pham, G. Verma, K. A. Forrest, B. Space, P. K. Thallapally, A. M. Al-Enizi and S. Ma, *Angew. Chem., Int. Ed.*, 2022, **61**, e202117807.

36 X. Li, D. Sensharma, W. Graham, V. Bon, E. Lin, X.-J. Kong, T. He, A. A. Bezrukov, Z. Zhang, S. Kaskel, T. Thonhauser and M. J. Zaworotko, *Angew. Chem., Int. Ed.*, 2025, **64**, e202507757.

37 B.-Q. Song, Q.-Y. Yang, S.-Q. Wang, M. Vandichel, A. Kumar, C. Crowley, N. Kumar, C.-H. Deng, V. GasconPerez, M. Lusi, H. Wu, W. Zhou and M. J. Zaworotko, *J. Am. Chem. Soc.*, 2020, **142**, 6896–6901.

38 M. Jung, J. Park, R. Muhammad, T. Park, S.-Y. Jung, J. Yi, C. Jung, J. Ollivier, A. J. Ramirez-Cuesta, J. T. Park, J. Kim, M. Russina and H. Oh, *Nat. Commun.*, 2025, **16**, 2032.

39 R. A. Klein, L. W. Bingel, A. Halder, M. Carter, B. A. Trump, E. D. Bloch, W. Zhou, K. S. Walton, C. M. Brown and C. M. McGuirk, *J. Am. Chem. Soc.*, 2023, **145**, 21955–21965.

40 Q. Dong, X. Zhang, S. Liu, R.-B. Lin, Y. Guo, Y. Ma, A. Yonezu, R. Krishna, G. Liu, J. Duan, R. Matsuda, W. Jin and B. Chen, *Angew. Chem., Int. Ed.*, 2020, **59**, 22756–22762.

41 R. M. Main, S. M. Vornholt, C. M. Rice, C. Elliott, S. E. Russell, P. J. Kerr, M. R. Warren and R. E. Morris, *Commun. Chem.*, 2023, **6**, 44.

42 W. M. Bloch, N. R. Champness and C. J. Doonan, *Angew. Chem., Int. Ed.*, 2015, **54**, 12860–12867.

43 T. L. Easun, F. Moreau, Y. Yan, S. Yang and M. Schröder, *Chem. Soc. Rev.*, 2017, **46**, 239–274.

44 M.-A. Springuel-Huet, A. Nossov, Z. Adem, F. Guenneau, C. Volkringer, T. Loiseau, G. Férey and A. Gédéon, *J. Am. Chem. Soc.*, 2010, **132**, 11599–11607.

45 P. L. Llewellyn, G. Maurin, T. Devic, S. Loera-Serna, N. Rosenbach, C. Serre, S. Bourrelly, P. Horcajada, Y. Filinchuk and G. Férey, *J. Am. Chem. Soc.*, 2008, **130**, 12808–12814.

46 C. X. Bezuidenhout, V. J. Smith, P. M. Bhatt, C. Esterhuysen and L. J. Barbour, *Angew. Chem., Int. Ed.*, 2015, **54**, 2079–2083.

47 H. Wang, M. Warren, J. Jagiello, S. Jensen, S. K. Ghose, K. Tan, L. Yu, T. J. Emge, T. Thonhauser and J. Li, *J. Am. Chem. Soc.*, 2020, **142**, 20088–20097.

48 J.-P. Zhang, P.-Q. Liao, H.-L. Zhou, R.-B. Lin and X.-M. Chen, *Chem. Soc. Rev.*, 2014, **43**, 5789–5814.

49 P. Lama, H. Aggarwal, C. X. Bezuidenhout and L. J. Barbour, *Angew. Chem., Int. Ed.*, 2016, **55**, 13271–13275.

50 E. J. Carrington, S. F. Dodsworth, S. van Meurs, M. R. Warren and L. Brammer, *Angew. Chem., Int. Ed.*, 2021, **60**, 17920–17924.

51 M. Đaković, M. Pisačić, M. Borovina, I. Kodrin, A. Kenđel and T. Frey, *J. Am. Chem. Soc.*, 2025, **147**, 22219–22227.

52 P. Lama and L. J. Barbour, *J. Am. Chem. Soc.*, 2018, **140**, 2145–2150.

53 X. Cui, K. Chen, H. Xing, Q. Yang, R. Krishna, Z. Bao, H. Wu, W. Zhou, X. Dong, Y. Han, B. Li, Q. Ren, M. J. Zaworotko and B. Chen, *Science*, 2016, **353**, 141–144.

54 B.-Q. Song, M.-Y. Gao, L. Mercene van Wyk, C.-H. Deng, A. C. Eaby, S.-Q. Wang, S. Darwish, D. Li, S.-J. Qin, Y.-L. Peng, Q.-Y. Yang, L. J. Barbour and M. J. Zaworotko, *Chem. Sci.*, 2025, **16**, 9010–9019.

55 L. Li, H.-M. Wen, C. He, R.-B. Lin, R. Krishna, H. Wu, W. Zhou, J. Li, B. Li and B. Chen, *Angew. Chem., Int. Ed.*, 2018, **57**, 15183–15188.

56 L. Yang, X. Cui, Z. Zhang, Q. Yang, Z. Bao, Q. Ren and H. Xing, *Angew. Chem., Int. Ed.*, 2018, **57**, 13145–13149.

57 Y.-L. Peng, C. He, T. Pham, T. Wang, P. Li, R. Krishna, K. A. Forrest, A. Hogan, S. Suepaul, B. Space, M. Fang, Y. Chen, M. J. Zaworotko, J. Li, L. Li, Z. Zhang, P. Cheng and B. Chen, *Angew. Chem., Int. Ed.*, 2019, **58**, 10209–10214.

58 L. Yang, X. Cui, Y. Zhang, Q. Yang and H. Xing, *J. Mater. Chem. A*, 2018, **6**, 24452–24458.

59 L. Yang, X. Cui, Q. Yang, S. Qian, H. Wu, Z. Bao, Z. Zhang, Q. Ren, W. Zhou and B. Chen, *Adv. Mater.*, 2018, **30**, 1705374.

60 L. Li, R.-B. Lin, R. Krishna, X. Wang, B. Li, H. Wu, J. Li, W. Zhou and B. Chen, *J. Am. Chem. Soc.*, 2017, **139**, 7733–7736.

61 B. Yu, S. Geng, H. Wang, W. Zhou, Z. Zhang, B. Chen and J. Jiang, *Angew. Chem., Int. Ed.*, 2021, **60**, 25942–25948.

62 A. L. Spek, *Acta Cryst. D*, 2009, **65**, 148–155.

63 M. A. Spackman and D. Jayatilaka, *CrystEngComm*, 2009, **11**, 19–32.

64 (*a*) CCDC 2044415: Experimental Crystal Structure Determination, 2026, DOI: 10.5517/ccdc.csd.cc26mcw3.; (*b*) CCDC 2044416: Experimental Crystal Structure Determination, 2026, DOI: 10.5517/ccdc.csd.cc26mcx4; (*c*) CCDC 2034435: Experimental Crystal Structure Determination, 2026, DOI: 10.5517/ccdc.csd.cc268zyf.